 CMC, vol.38, no.2, pp.105-128, 2013

Theoretical Simulation of AlN Nanobelts and Nanorings

Aurora Costales[1], C. J. F. Solano[2], E. Francisco[1] and A. Martín Pendás[1]

Abstract: An extension of our previously reported periodic cluster model (*J. Phys. Chem. C* **2008**, 112, 6667-6676) to nanorings and nanobelts is presented. This new scheme allows for accurately calculating reasonably large nanostructures while preserving a very small number of optimization parameters. The model has been applied to a number of AlN semiconducting structures using *ab initio* pair potentials. Attention has been paid to the variation of the B1-B4 phase transition pressure as the the size of the structures is varied.

Keywords: nanorings, nanobelts, nanocrystals, III-V semiconductor

1 Introduction

The theoretical and experimental study of nanocrystals has arisen a great interest in recent times due to the large variety of properties that they have, many of them of great technological importance. From the experimental point of view, the ability to make a high quality nanocrystal, controlling its size, shape, the number and kind of its defects, the surface design, etc, is key to this area of science and technology. For instance, by tuning the size of the nanostructures of a given compound one can achieve very different values for many properties. Hence, investigating the size dependence of these properties is very relevant both from a practical and theoretical point of view.

A large number of experimental works have been done [Alivisatos (1996); Wang, Tait, Zhao, Schiferl, Zha, Uchida and Downs (2004); Kao, Bai, Lucas, Alivisatos and Ting (2013); Beberwyck and Alivisatos (2012); Choi and Alivisatos (2010)] in this field in order to cast nanostructures with specific properties. However, theoretical simulations that could help to direct the synthesis of nanostructures are scarce[Morgan and Madden (2004); Kodiyalam, Kalia, Nakano and Vashishta

[1] Departamento de Química Física y Analítica. Facultad de Química, Universidad de Oviedo, 33006-Oviedo, Spain.

[2] Laboratory for Chemistry of Novel Materials, University of Mons, Place du Parc 20, 7000 Mons, Belgium.

(2004); Grünwald, Rabani, and Dellago (2004); Morgan and Madden (2006); Morgan and Madden (2006b); Grünwald, Dellago and Geissler (2007); Morgan (2010)] mainly due to their high computational cost, that grows dramatically with the size of the nanostructure.

In order to partially avoid this problem, we presented a few years ago the periodic cluster model [Costales, Blanco, Francisco, Solano and Martín Pendás (2008); Francisco (2004)], a theoretical scheme aimed to perform theoretical simulations of nanocrystals. One the fundamental tasks that is necessary to carry out in this type of research is to locate the geometrical arrangement of the atoms giving rise to the minimum possible value of the energy. In principle, the computational cost for the search of this minimum energy structure increases *exponentially* with the number of degrees of freedom. The basic tenet of the periodic cluster model is to reduce the dimensionality of the configuration space using the periodicity displayed by nanocrystals while maintaining the finiteness of the system. Although the model can be applied using highly-accurate quantum mechanical methods as well other less accurate or semiempirical ones, in practice one is forced to trade some accuracy in in favor of reaching the large-size nanoscale limit, so that most accurate electronic structure methods cannot cope with such system sizes and more simplified schemes need to be used to evaluate the energy of a given nanocrystalline configuration.

In this article, an extension of the periodic cluster model is introduced which allows us to simulate nanobelts and nanorings. Since AlN is a technologically important material (see e.g. Refs. [Nakamura (1996); Belyanin, Bouilov, Zhirnov, Kamenev, Kovalskiji and Spitsyn (1999); Serrano, Rubio, Hernández, Muñoz and Mújica (2000)]) in which our group has previous experience [Kandalam, Blanco and Pandey (2002); Costales, Blanco, Martín Pendás, Kandalam and Pandey (2002); Costales, Kandalam and Pandey (2003); Costales, Blanco, Francisco, Pandey and Martín Pendás (2005); Costales, Blanco, Francisco, Martín Pendás and Pandey (2006)], different nanobelts and nanorings of AlN have been selected to be simulated using this extension of the periodic cluster model.

The rest of the article is organized as follows. Section 2 presents our simulation methodology, including the extension of the periodic cluster model. Section 3 presents the results of our simulations on AlN nanobelts and nanorings. Finally, Section 4 presents our main conclusions.

2 Methodology

The simulation methodology employed in this work comprises two main pieces. First, the well known pair potential scheme to evaluate the energy of a given con-

figuration. Second, an extension of the periodic cluster model for selection of configurations in nanobelts and nanorings, in which the energetics of the surface termination is included without its geometric complexities. For the sake of completeness, a brief description of the periodic cluster model is also included.

2.1 Pair potentials for nanostructure simulations

Ab initio quantum mechanical methods are the more precise schemes to simulating the properties of materials. However, large nanostructures cannot be modelled in more than a few configurations (if any) using these sophisticated methods. Hence, simplified schemes are key in the understanding of the nanoscale, and atomistic simulations using n–body potentials become next in accuracy after quantum mechanics methods.

In atomistic simulations using pair potentials [Born and Mayer (1932); Huggins and Mayer (1933); Mayer and Levy (1933)], the (binding) energy of a system can be computed as a sum of pair potential interatomic interactions,

$$E = \sum_i \sum_{j<i} E_{ij}, \tag{1}$$

where E_{ij} is the pair potential between atoms i and j. For the sake of simplicity, E_{ij} is assumed to be central (i. e. $E_{ij} = E_{ij}(r_{ij})$) although polarization effects can be incorporated in various ways (for example, see Ref. [Dick and Overhauser (1958)]).

In nanostructures whose bonds have important ionic contributions, one further assumes that the system is composed by ions and that a high percentage of the (binding) energy is due to Coulomb interactions. Thus, E_{ij} can be written as

$$E_{ij} = \frac{q_i q_j}{r_{ij}} + V_{ij}(r_{ij}), \tag{2}$$

where q_i and q_j are ionic charges, r_{ij} the interatomic distance between ions i and j, and $V_{ij}(r_{ij})$ a short-range potential which is repulsive at short distances and rapidly decays to zero when r_{ij} increases.

2.2 The Periodic Cluster model

Even under the assumption of pairwise additivity of central potentials, the problem of exploring the potential energy surface to select lowest-energy configurations is still an enormous task even for medium-sized nanoparticles [Costales, Blanco, Francisco, Pandey and Martín Pendás (2005)]. Although the energy evaluation for a given configuration can still be achievable, the number of degrees of freedom,

roughly $3N_{tot}$ (N_{tot} being the total number of atoms), becomes so large that either (i) the convergence of energy minimizations is very slow if gradient-only techniques are used, or (ii) the size of the problem becomes easily intractable if quadratic-convergence Hessian matrix optimization techniques are used. Thus, even a single optimization run is a troublesome task, and global optimizations are out of reach. In the simulation of solids and liquids, these dimensionality problems are solved by using periodic boundary conditions and an infinite size assumption: in the solid, the crystalline structure displays indeed a unit cell that is replicated in the three dimensions, while in the liquid the simulation cell is taken as large as possible so that this replication does not affect the average properties. However, the problem is different in nanosystems, where the size is necessarily finite. Even in nanocrystals, where the experimental structure displays some degree of long-range order, it is the frontier effects that distinguish them from solid crystals, and hence an infinite replication scheme cannot be used.

In order to avoid these problems, the Periodic Cluster (PC) model [Costales, Blanco, Francisco, Solano and Martín Pendás (2008); Francisco (2004)] has been developed and implemented in the *cluster* code [Francisco (2005)]. An ideal crystal is formed by an infinite repetition of a unit cell along the directions determined by the lattice vectors $\vec{a}$, $\vec{b}$ and $\vec{c}$. Let us write the transpose vector position of the unit cell n with respect to a reference unit cell as $\mathbf{l}_n^t = (l_{n1}\, l_{n2}\, l_{n3})$, where l_{n1}, l_{n2} and l_{n3} are integers. A *periodic cluster* is defined as a fragment of the ideal infinite crystal where $l_{n1} \in [0, N_a - 1]$, $l_{n2} \in [0, N_b - 1]$, and $l_{n3} \in [0, N_c - 1]$, being N_a, N_b, and N_c the maximum number of cells in the directions of the crystallographic axes Oa, Ob, and Oc, respectively. Further, one assumes that the fractional position of atom i within the unit cell (all of its components lie in the range $[0,1)$), $\mathbf{u}_i^t = (u_{i1}\, u_{i2}\, u_{i3})$, is identical in different unit cells. Thereby, the position of atom i belonging to the n unit cell of the periodic cluster is given by

$$\mathbf{x}_{in} = \mathbf{u}_i + \mathbf{l}_n. \tag{3}$$

In turn, the interatomic distance between atoms i and j, that belong to unit cells n and m, respectively, $r_{in,jm}$, can be obtained from

$$r_{in,jm}^2 = \mathbf{x}_{in,jm}^t \mathbf{G} \mathbf{x}_{in,jm}, \tag{4}$$

where

$$\mathbf{x}_{in,jm} = \mathbf{x}_{jm} - \mathbf{x}_{in}, \tag{5}$$

and

$$\mathbf{G} = \begin{pmatrix} \vec{a}\cdot\vec{a} & \vec{a}\cdot\vec{b} & \vec{a}\cdot\vec{c} \\ \vec{b}\cdot\vec{a} & \vec{b}\cdot\vec{b} & \vec{b}\cdot\vec{c} \\ \vec{c}\cdot\vec{a} & \vec{c}\cdot\vec{b} & \vec{c}\cdot\vec{c} \end{pmatrix} = \begin{pmatrix} a^2 & ab\cos\gamma & ac\cos\beta \\ ba\cos\gamma & b^2 & bc\cos\alpha \\ ca\cos\beta & cb\cos\alpha & c^2 \end{pmatrix} \tag{6}$$

is the metric tensor. Because (l_{n1}, l_{n2}, l_{n3}) are fixed values, the interatomic distance $r_{in,jm}$ only depends on both the lattice paramaters $(a,b,c,\alpha,\beta,\gamma)$ and the fractional positions (u_{i1}, u_{i2}, u_{i3}) and (u_{j1}, u_{j2}, u_{j3}).

In this way, the periodic cluster (binding) energy can be described as

$$E = \sum_{n>m} \sum_{i\in n} \sum_{j\in m} \left[\frac{q_i q_j}{r_{in,jm}} + V_{ij}(r_{in,jm}) \right] + \sum_{n} \sum_{i>j} \left[\frac{q_i q_j}{r_{in,jn}} + V_{ij}(r_{in,jn}) \right]. \quad (7)$$

In Eq. 7, the first term only includes pair potentials between atoms that belong to different unit cells while the second term only consideres pair potentials between atoms in the same unit cell. Since all the unit cells are equivalent, the second term can be written as

$$\sum_{n} \sum_{i>j} \left[\frac{q_i q_j}{r_{in,jn}} + V_{ij}(r_{in,jn}) \right] = N_{cell} \sum_{i>j} \left[\frac{q_i q_j}{r_{i0,j0}} + V_{ij}(r_{i0,j0}) \right], \quad (8)$$

where $r_{i0,j0}$ is the interatomic distance between the atoms i and j in the reference unit cell, and $N_{cell} = N_a N_b N_c$ is the total number of unit cells in the periodic cluster. Let us denote the total number of atoms in a unit cell as $\mathscr{N}$. The periodic cluster (binding) energy depends only on $3\mathscr{N}+6$ variables, which are the fractional positions, (u_{i1}, u_{i2}, u_{i3}) where $i = 1, ..., \mathscr{N}$, as well as the lattice paramaters $(a,b,c,\alpha,\beta,\gamma)$. Since $\mathscr{N} << N_{tot} = \mathscr{N} N_{cell}$, the periodic cluster model drastically reduces the number of variables that need to be taken into account in the optimizations. Further restrictions in these variables may be adopted, perhaps to maintain the symmetry features displayed by the bulk crystal structure in the simulated periodic cluster, with a further reduction of the number of optimizable parameters.

In summary, the PC model corresponds to minimizing the energy of the unit cells subjected to a kind of average Madelung potential obtained from considering all their possible different spatial environments. Although mixed models can be devised in which the frontier cells are allowed to lose part or all of their periodicity, these have not been included in the initial implementation of this model.

2.3 Extension of the Periodic Cluster model for nanobelts and nanorings

An extension of the periodic cluster model has been implemented in the *cluster* code [Solano (2009)] so that nanobelts and nanorings can be simulated. A *nanobelt* is a periodic cluster in which one dimension is much larger than the other two. From a *self-coiling* process [Kong, Ding, Yang and Wang (2004); Duan, Yang, Liu, Gong, Huang, Zhao, Tang, Zhang and Du (2005); Wang (2004)], a *nanoring* can be obtained from the corresponding nanobelt. Since both nanostructures are each other related, it would be reasonable to describe nanobelts and nanorings using reference systems in which the degrees of freedom of the binding energy are described

using common variables. To this end, some transformations will be applied on the periodic cluster coordinates. First,the atomic coordinates for a periodic cluster in the orthonormal basis $(\vec{i},\vec{j},\vec{k})$ are given by the linear transformation

$$\mathbf{x}_{in}^{or} = \mathbf{R}\mathbf{x}_{in}, \tag{9}$$

where $\mathbf{x}_{in}$ is defined in Eq. 3 and the matrix $\mathbf{R}$ is given by

$$\mathbf{R} = \begin{pmatrix} a & b\cos\gamma & c\cos\beta \\ 0 & b\sin\gamma & c\frac{\cos\alpha-\cos\beta\cos\gamma}{\sin\gamma} \\ 0 & 0 & \frac{V}{ab\sin\gamma} \end{pmatrix}, \tag{10}$$

V being the unit cell volume. In this transformation, the orthonormal basis $(\vec{i},\vec{j},\vec{k})$ satisfies the following properties: (i) the unitary vector $\vec{i}$ is parallel to the lattice vector $\vec{a}$; (ii) the unitary vector $\vec{j}$ belongs to the plane defined by the lattice vector $(\vec{a},\vec{b})$; and (iii) $\vec{j}\cdot\vec{b}$ and $\vec{k}\cdot\vec{c}$ are positive real numbers. Second, a linear transformation

$$\mathbf{x}_{in}^{par} = \mathbf{T}\mathbf{x}_{in}^{or} \tag{11}$$

is applied on the previous cartesian coordinates, where the matrix $\mathbf{T}$ is given by

$$\mathbf{T} = \begin{pmatrix} \frac{1}{L} & 0 & 0 \\ 0 & \frac{1}{W} & 0 \\ 0 & 0 & \frac{1}{T} \end{pmatrix}, \tag{12}$$

with $L = N_a a$, $W = N_b b\sin\gamma$, and $T = N_c V/(ab\sin\gamma)$. Notice that LWT is equal to the periodic cluster volume. If one arbitrarily imposes $N_a \gg N_b > N_c$, L is related to the periodic cluster length, and W and T are related to the periodic cluster width and thickness, respectively. By substituting Eq. 9 into Eq. 11, one obtains

$$\mathbf{x}_{in}^{par} = \mathbf{T}\mathbf{R}\mathbf{x}_{in} = \mathbf{A}\mathbf{x}_{in}, \tag{13}$$

where matrix $\mathbf{A}$ is given by

$$\mathbf{A} = \begin{pmatrix} \frac{1}{N_a} & \frac{r_1}{N_a} & \frac{r_2}{N_a} \\ 0 & \frac{1}{N_b} & \frac{r_3}{N_b} \\ 0 & 0 & \frac{1}{N_c} \end{pmatrix}, \tag{14}$$

and $r_1 = b\cos\gamma/a$, $r_2 = c\cos\beta/a$, and $r_3 = c(\cos\alpha - \cos\beta\cos\gamma)/(b\sin^2\gamma)$. Although there is a non-linear relation between the lattice parameters and the (L,W,T,r_1,r_2,r_3) set, the unit cell can also be described with the latter ones.

The atomic coordinates given by Eq. 13 are the initial point for the transformation which allows to describe the positions for nanobelts and nanorings. For periodic nanobelts, one uses the linear transformation given by

$$\mathbf{x}_{in}^{belt} = \mathbf{T}^{-1}\mathbf{x}_{in}^{par} = \begin{pmatrix} Lx_{in}^{par} \\ Wy_{in}^{par} \\ Tz_{in}^{par} \end{pmatrix}. \tag{15}$$

Note that $\mathbf{x}_{in}^{belt} = \mathbf{x}_{in}^{or}$, but the (L,W,T,r_1,r_2,r_3) variables are used for describing the unit cell. For periodic nanorings, one uses a non-linear transformation given by

$$\mathbf{x}_{in}^{ring} = \begin{pmatrix} r_{in}\cos\theta_{in} \\ y_{in}^{ring} \\ r_{in}\sin\theta_{in} \end{pmatrix} = \begin{pmatrix} (R+Tz_{in}^{par})\cos 2\pi x_{in}^{par} \\ Wy_{in}^{par} \\ (R+Tz_{in}^{par})\sin 2\pi x_{in}^{par} \end{pmatrix}, \tag{16}$$

where the Oy axis is selected perpendicular to the nanoring plane, and $(r_{in}, y_{in}^{ring}, \theta_{in})$ are cylindrical coordinates and $R = L/(2\pi)$ is the nanoring internal radius. Note that the vector spaces spanned by the initial orthogonal basis and the final orthonormal basis are not the same and that, therefore, the map described by Eq. 16 is not a coordinate transformation.

From Eq. 15 and Eq. 16, the interatomic distances between atoms i and j belonging to n and m unit cells, $r_{in,jm}$, can be obtained from

$$r_{in,jm}^2 = \left(\mathbf{x}_{in,jm}^{nano}\right)^t \mathbf{x}_{in,jm}^{nano}, \tag{17}$$

where

$$\mathbf{x}_{in,jm}^{nano} = \mathbf{x}_{jm}^{nano} - \mathbf{x}_{in}^{nano} \tag{18}$$

and $nano = \{belt, ring\}$. As described above, the periodic cluster (binding) energy depends only on $3\mathcal{N}+6$ variables, but the lattice parameters are now replaced by the (L,W,T,r_1,r_2,r_3) variables.

3 Local optimizations of AlN periodic nanobelts and nanorings

We are interested in the B4 and B1 crystal phases of AlN. the B4 bulk phase ($P6_3mc$ spacial group) is stable at room temperature while the B1 bulk phase ($Fm\bar{3}m$ spacial group) is stable at high pressures. In our previous AlN nanocluster optimizations [Costales, Blanco, Francisco, Pandey and Martín Pendás (2005); Costales, Blanco, Francisco, Martín Pendás and Pandey (2006)], the short-range potential has been modeled through

$$V_{ij}(r) = \sum_m A_m^{ij} r_m^{n_m^{ij}} e^{-\rho_m^{ij} r}, \tag{19}$$

Table 1: A_m^{ij}, n_m^{ij}, and ρ_m^{ij} parameters for the short-range potential. Atomic units are used.

$i-j$	A_1^{ij}	n_1^{ij}	ρ_1^{ij}	A_2^{ij}	n_2^{ij}	ρ_2^{ij}
Al–N	100.458815	0	2.182429			
Al–Al	−41.557010	0	1.171765	60.196250	−1	0.924620
N–N	84.586517	1	2.042769	−151.886016	3	2.995922

where the A_m^{ij}, n_m^{ij}, and ρ_m^{ij} parameters are described in Tab. 1. Further, Al and N charges are set equal to +2 and -2, respectively. As shown in the AlN nanocrystal optimizations [Costales, Blanco, Francisco, Solano and Martín Pendás (2008)], conventional (Z=4) and orthogonal ($\alpha=\beta=\gamma=90^0$) unit cells are the best option for describing B4-like and B1-like AlN nanostructures. As indicated in the previous section, we use an arbitrary selection in which the *Oa* axis is related to the nanostructure length, the *Ob* axis is related to the nanostructure width, and the *Oc* axis is related to the nanostructure thickness. For B1-like AlN periodic nanobelts and nanorings, the initial cubic ($a=b=c$) unit cell is used in our optimizations. For B4-like AlN periodic nanobelts and nanorings, the initial orthorhombic ($a\neq b\neq c$) unit cell is obtained from a transformation of the hexagonal primitive unit cell in which the new axes are $2\vec{a}+\vec{b}$, $\vec{c}$ and $-\vec{b}$. Thereby, the permanent dipolar moment is oriented along the *Ob* axis. These new axes are those in experimental nanobelts and nanorings [Kong, Ding, Yang and Wang (2004)]. Further, the fractional positions for Al atoms are $(\frac{1}{6}\,0\,\frac{1}{2})$, $(\frac{1}{3}\,\frac{1}{2}\,0)$, $(\frac{2}{3}\,0\,0)$, $(\frac{5}{6}\,\frac{1}{2}\,\frac{1}{2})$, and $(\frac{1}{6}\,\frac{1}{2}+z_N\,\frac{1}{2})$, $(\frac{1}{3}\,z_N\,0)$, $(\frac{2}{3}\,\frac{1}{2}+z_N\,0)$, $(\frac{5}{6}\,z_N\,\frac{1}{2})$ for N atoms, where $z_N=0.1098$[1]. To maintain the symmetry features displayed by the bulk crystal structure in the simulated nanostructures, (L,W,T) are unrestricted variables for B4-like and B1-like AlN periodic nanobelt and nanoring optimizations. Because the unit cell is orthogonal for both B4-like and B1-like periodic nanobelts and nanorings, the (binding) energy optimization which depends on the (L,W,T) unrestricted variables is equivalent to the (binding) energy optimization which depends on the (a,b,c) lattice parameters. Additionally, the z_N parameter is also an unrestricted variable for B4-like AlN periodic nanobelt and nanoring optimizations. The Memory Limited Broyden-Fletcher-Goldfarb-Shano (LBFGS) optimization algorithm [Liu and Nocedal (1989)] has been used. This is a modification of the Davidon-Fletcher-Powell (DFP) method implemented by Jorge Nocedal [Nocedal (1980)].

The optimized lattice parameters for B4-like and B1-like AlN nanobelts are shown

[1] the z_N value is obtained from AlN pair potentials simulations for the B4 crystal structure using a hexagonal primitive unit cell. This value is close to the experimental value, $z_N=0.1128$.

Table 2: Optimized lattice parameters for B4-like and B1-like AlN nanobelts for $N_a = 200$.

		B4			B1		
N_b	N_c	a (a_0)	b (a_0)	c (a_0)	a (a_0)	b (a_0)	c (a_0)
1	1	9.7100	6.7846	5.4842	6.5516	7.2071	7.2071
2	1	10.0535	6.7843	5.6502	6.7216	7.1506	7.3586
3	1	10.2116	6.7597	5.7260	6.7974	7.1105	7.4256
4	1	10.3029	6.7437	5.7697	6.8407	7.0865	7.4639
5	1	10.3626	6.7329	5.7983	6.8689	7.0708	7.4888
1	2	9.8163	7.0432	5.7293	6.7216	7.1506	7.3586
2	2	10.1056	7.0226	5.8669	6.8776	7.2978	7.2978
3	2	10.2364	6.9909	5.9284	6.9468	7.2538	7.3630
4	2	10.3112	6.9710	5.9636	6.9864	7.2273	7.4002
5	2	10.3599	6.9578	5.9865	7.0122	7.2100	7.4244
1	3	9.8748	7.1691	5.7529	6.7974	7.1105	7.4256
2	3	10.1368	7.1358	5.8848	6.9468	7.2538	7.3630
3	3	10.2543	7.1002	5.9434	7.0132	7.3173	7.3173
4	3	10.3212	7.0781	5.9770	7.0511	7.2897	7.3536
5	3	10.3647	7.0635	5.9988	7.0757	7.2716	7.3771
1	4	9.9041	7.2425	5.7602	6.8407	7.0865	7.4639
2	4	10.1514	7.2017	5.8885	6.9864	7.2273	7.4002
3	4	10.2616	7.1638	5.9455	7.0511	7.2897	7.3536
4	4	10.3246	7.1404	5.9780	7.0881	7.3254	7.3254
5	4	10.3655	7.1250	5.9991	7.1121	7.3069	7.3485
1	5	9.9215	7.2906	5.7633	6.8689	7.0708	7.4888
2	5	10.1596	7.2451	5.8893	7.0122	7.2100	7.4244
3	5	10.2656	7.2055	5.9451	7.0757	7.2716	7.3771
4	5	10.3260	7.1814	5.9770	7.1121	7.3069	7.3485
5	5	10.3652	7.1654	5.9976	7.1356	7.3298	7.3298

in Tab. 2 for $N_a = 200$ and for different N_b and N_c values. B1-like AlN optimized nanobelts have the same values for the lattice parameters when one interchanges the N_a and N_b values. Due to the equivalence of the three space directions for B1-like nanobelts, a different spatial orientation is achieved if one interchanges the N_a and N_b values, but the structure remains unchanged. Additionally, $z_N \simeq 0$ is found for B4-like AlN optimized nanobelts (and nanorings) so that the permanent dipolar moment is mitigated. Hence, B_k-like AlN nanobelts (and nanorings) are obtained from the initial B4-like AlN nanobelts (and nanorings) after (binding) energy opti-

Table 3: Optimized lattice parameters for B4-like and B1-like AlN nanorings for $N_a = 200$.

		B4			B1		
N_b	N_c	a (a_0)	b (a_0)	c (a_0)	a (a_0)	b (a_0)	c (a_0)
1	1	9.6671	6.7873	5.4846	6.4972	7.2116	7.2084
2	1	10.0093	6.7862	5.6503	6.6661	7.1539	7.3590
3	1	10.1668	6.7614	5.7259	6.7414	7.1136	7.4257
4	1	10.2577	6.7453	5.7696	6.7844	7.0895	7.4637
5	1	10.3172	6.7344	5.7981	6.8124	7.0737	7.4884
1	2	9.6862	7.0462	5.7277	6.5693	7.3574	7.1404
2	2	9.9726	7.0244	5.8652	6.7231	7.2960	7.2870
3	2	10.1019	6.9925	5.9267	6.7915	7.2519	7.3520
4	2	10.1759	6.9725	5.9619	6.8306	7.2254	7.3891
5	2	10.2241	6.9592	5.9848	6.8560	7.2080	7.4132
1	3	9.6605	7.1714	5.7498	6.5579	7.4170	7.0857
2	3	9.9181	7.1368	5.8816	6.7051	7.3540	7.2285
3	3	10.0335	7.1008	5.9403	6.7705	7.3083	7.2918
4	3	10.0995	7.0786	5.9738	6.8080	7.2807	7.3279
5	3	10.1423	7.0639	5.9956	6.8323	7.2626	7.3513
1	4	9.6081	7.2431	5.7551	6.5238	7.4458	7.0439
2	4	9.8500	7.2010	5.8835	6.6678	7.3819	7.1842
3	4	9.9580	7.1626	5.9404	6.7319	7.3353	7.2464
4	4	10.0197	7.1391	5.9730	6.7686	7.3071	7.2819
5	4	10.0592	7.1240	5.9940	6.7925	7.2886	7.3050
1	5	9.5463	7.2887	5.7559	6.4834	7.4593	7.0077
2	5	9.7784	7.2417	5.8820	6.6262	7.3948	7.1465
3	5	9.8818	7.2018	5.9379	6.6899	7.3476	7.2080
4	5	9.9411	7.1774	5.9698	6.7263	7.3190	7.2432
5	5	9.9792	7.1614	5.9906	6.7501	7.3003	7.2660

mizations using the (L,W,T,z_N) unrestricted set of variables. As discussed in our previous papers [Costales, Blanco, Francisco, Solano and Martín Pendás (2008); Solano, Costales, Francisco, Martín Pendás, Blanco, Lau, He and Pandey (2008)], the energy ordering of B4 and B_k may change in finite systems. It seems reasonable that the lattice parameters of B4-like and B1-like AlN nanobelts should tend to the ideal crystal values in the macroscopic limit $(N_a \to \infty, N_b \to \infty, N_c \to \infty)$. For B1-like AlN nanobelts, the lattice parameters exhibit this tendency when the

N_a, N_b and N_c parameters are increased[2]. For B4-like AlN nanobelts, the a and c lattice parameters also exhibit this tendency when the N_a, N_b, and N_c parameters are increased[3]. However, the b parameter has values far from the ideal crystal value if one compares with the behavior shown by a and c parameters. This is because B_k-like nanobelts are obtained from optimizations of B4-like nanobelts and the b parameter for the B_k structure is smaller than the b parameter for the B4 structure. In Tab. 3, the optimized lattice parameters for B4-like and B1-like AlN nanorings are shown for $N_a = 200$ and different N_b and N_c values. The behavior shown by the lattice parameters of nanorings is analogous to that described for nanobelts.

In Fig. 1 and Fig. 2, the energy per unit formula $\bar{E} = (E/(ZN_{cell}))$ vs N_a^{-1} is depicted for B4-like and B1-like AlN nanobelts, respectively. $\bar{E}$ shows a linear behavior which may be fitted through

$$\bar{E}(N_a,N_b,N_c) = \bar{E}(\infty,N_b,N_c) + \frac{A(N_b,N_c)}{N_a}, \tag{20}$$

where $\bar{E}(\infty,N_b,N_c)$ is the (binding) energy for a one-dimensional crystal and $A(N_b,N_c)$ a fitting parameter. In Tab. 4, the $\bar{E}(\infty,N_b,N_c)$ values are shown for B4-like and B1-like AlN nanobelts, respectively. As N_b and N_c increase $\bar{E}(\infty,N_b,N_c)$ tends to the ideal crystal energy[4]. To demonstrate this the binding energy tends to the ideal crystal energy in the macroscopic limit ($N_a \to \infty, N_b \to \infty, N_c \to \infty$), we obtain the (binding) energy for a two-dimensional crystal, $\bar{E}(\infty,\infty,N_c)$, from $\bar{E}(\infty,N_b,N_c)$ by means of polynomial fit given by

$$\bar{E}(\infty,N_b,N_c) = \bar{E}(\infty,\infty,N_c) + \frac{\alpha(N_c)}{N_b} + \frac{\beta(N_c)}{N_b^2}, \tag{21}$$

with $\alpha(N_c)$ and $\beta(N_c)$ being fitting parameters. Similarly, $\bar{E}(\infty,N_b,\infty)$ should be obtained from

$$\bar{E}(\infty,N_b,N_c) = \bar{E}(\infty,N_b,\infty) + \frac{\gamma(N_b)}{N_c} + \frac{\eta(N_b)}{N_c^2}, \tag{22}$$

where $\gamma(N_b)$ and $\eta(N_b)$ are fitting parameters. Then, the ideal crystal energy,

[2] From AlN pair potentials simulations for B1 crystal, the optimized lattice parameters are the $a = b = c = 7.3471\,a_0$.

[3] From AlN pair potentials simulations for B4 crystal, the optimized lattice parameters are $a = 10.1924\,a_0$, $b = 9.4093\,a_0$, and $c = 5.8864\,a_0$.

[4] Crystal energies are $-1.6465\,E_h$ and $-1.6428\,E_h$ for AlN pair potentials simulations for B4 and B1 crystal structure, respectively.

$\bar{E}(\infty,\infty,\infty) \equiv \bar{E}(crystal)$, is obtained from

$$\bar{E}(\infty,\infty,N_c) = \bar{E}(crystal) + \frac{\Gamma_1(N_c)}{N_b} + \frac{\Gamma_2(N_c)}{N_b^2}, \quad (23)$$

$$\bar{E}(\infty,N_b,\infty) = \bar{E}(crystal) + \frac{\Delta_1(N_b)}{N_c} + \frac{\Delta_2(N_b)}{N_c^2}, \quad (24)$$

where $\Gamma_1(N_c)$, $\Gamma_2(N_c)$, $\Delta_1(N_b)$, and $\Delta_2(N_b)$ are again fitting parameters. In this way, the values for the ideal crystal energy for the B4 (or more accurately the B_k) crystal structure are $-1.6475\,E_h$ and $-1.6476\,E_h$ as obtained with data taken from *Oxy* and *Oxz* infinite planes, respectively. This should be compared to the value for the ideal crystal energy found the B1 crystal structure: $-1.6422\,E_h$[5]. In view of these results, we may say that there is good agreement between extrapolated and bulk crystalline energies. nanostructures and the crystal energies for AlN pair potentials simulations for crystal structure (differences between them are smaller than $1\,mE_h$).

Table 4: $\bar{E}(\infty,N_b,N_c)$ values for B4-like and B1-like AlN nanobelts.

$\bar{E}(\infty,N_b,N_c)$ (E_h)				$\bar{E}(\infty,N_b,N_c)$ (E_h)			
N_b	N_c	B4	B1	N_b	N_c	B4	B1
1	1	-1.5588	-1.6091	4	1	-1.6017	-1.6275
1	2	-1.5942	-1.6202	4	2	-1.6201	-1.6319
1	3	-1.6077	-1.6248	4	3	-1.6274	-1.6341
1	4	-1.6148	-1.6275	4	4	-1.6313	-1.6353
1	5	-1.6191	-1.6288	4	5	-1.6337	-1.6361
2	1	-1.5856	-1.6202	5	1	-1.6051	-1.6288
2	2	-1.6103	-1.6272	5	2	-1.6223	-1.6330
2	3	-1.6199	-1.6302	5	3	-1.6291	-1.6350
2	4	-1.6249	-1.6319	5	4	-1.6328	-1.6361
2	5	-1.6280	-1.6330	5	5	-1.6350	-1.6369
				5	6	-1.6366	-1.6374
3	1	-1.5962	-1.6248	6	1		-1.6299
3	2	-1.6167	-1.6302	6	2		-1.6337
3	3	-1.6248	-1.6327	6	3		-1.6356
3	4	-1.6291	-1.6341	6	4		-1.6367
3	5	-1.6317	-1.6350	6	5		-1.6374

[5] Note that the *Oxy* and *Oxz* infinite planes are equivalents in B1-like AlN nanobelts and nanorings.

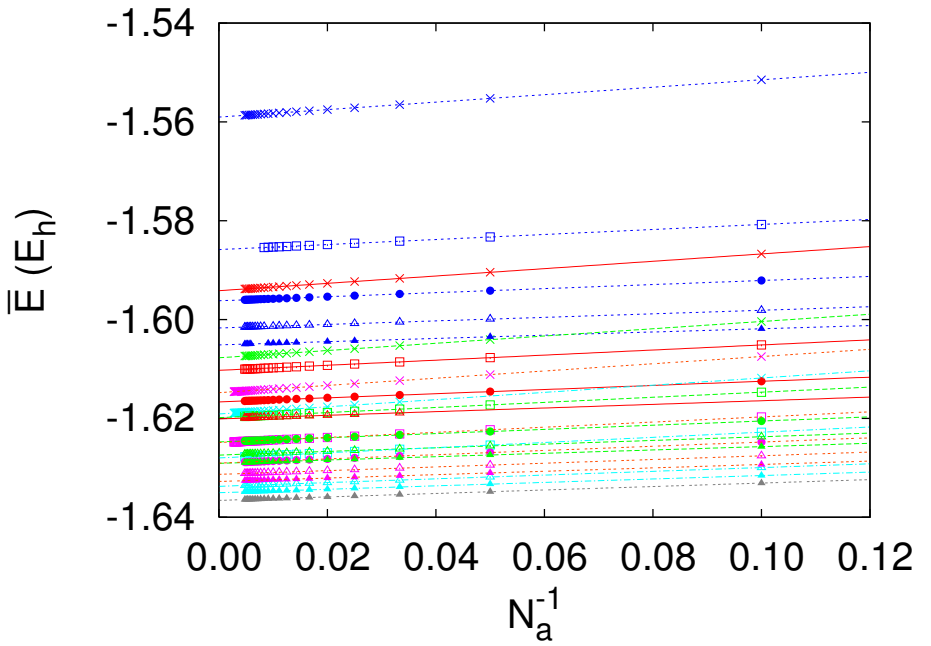

Figure 1: $\bar{E}$ vs N_a^{-1} for B4-like AlN nanobelts. The different N_c values are represented using different colors, so that dark blue is selected for $N_c = 1$, red for $N_c = 2$, green for $N_c = 3$, magenta for $N_c = 4$, light blue for $N_c = 5$, and gray for $N_c = 6$. The different N_b values are represented using different symbols, so that $\times$ symbol is used for $N_b = 1$, $\square$ for $N_b = 2$, $\bullet$ for $N_b = 3$, $\triangle$ for $N_b = 4$, $\blacktriangle$ for $N_b = 5$, and $\blacklozenge$ for $N_b = 6$. The same convention for colours and symbols will be used in the rest of figures (Fig. 2-Fig. 8).

In Fig. 3 and Fig. 4, $\bar{E}$ vs N_a^{-1} is depicted for B4-like and B1-like AlN nanorings, respectively. $\bar{E}$ shows a non-linear behavior that can be fitted using

$$\bar{E}(N_a,N_b,N_c) = \bar{E}(\infty,N_b,N_c) + \frac{A(N_a,N_b)}{N_a} + \frac{B(N_a,N_b)}{N_a^2} + \frac{C(N_b,N_c)}{N_a^3} + \frac{D(N_a,N_b)}{N_a^4}, \tag{25}$$

where $A(N_a,N_b)$, $B(N_a,N_b)$, $C(N_a,N_b)$, and $D(N_a,N_b)$ are fitting parameters. Although we have tested different analytical expressions to fit $\bar{E}(N_a,N_b,N_c)$ (as shown in Ref. [Hill (1994)] for colloidal particles), the above equation exhibits the best results for the ideal crystal energy. Further, the N_a^{-2}, N_a^{-3}, and N_a^{-4} terms can be related to the superficial energy contribution (i.e., the energy contribution related

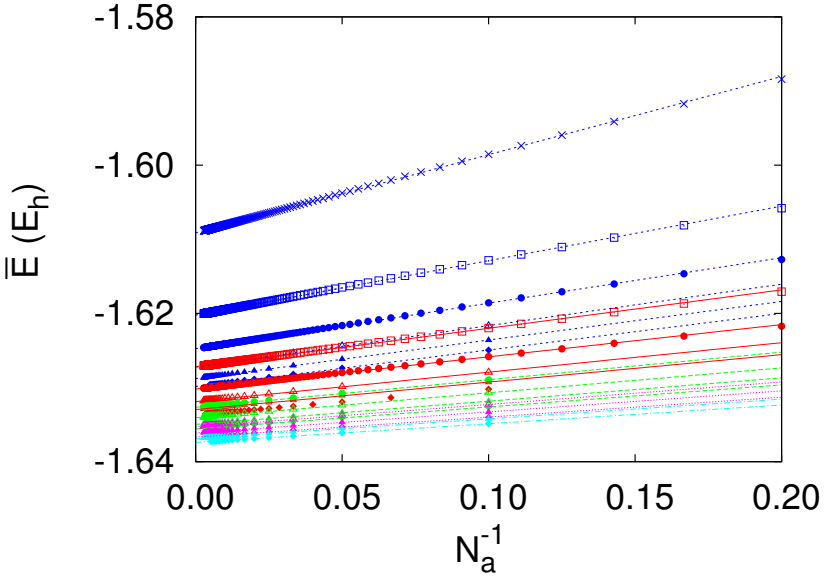

Figure 2: $\bar{E}$ vs N_a^{-1} for B1-like AlN nanobelts.

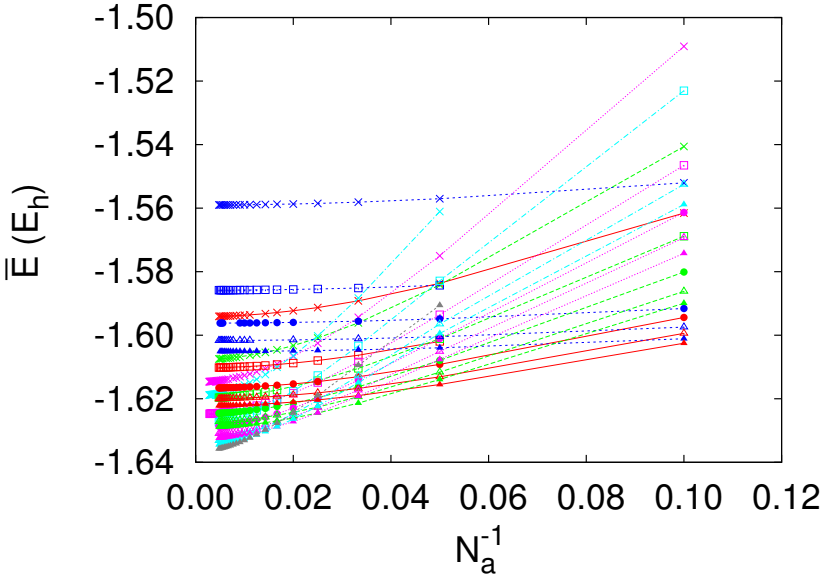

Figure 3: $\bar{E}$ vs N_a^{-1} for B4-like AlN nanorings.

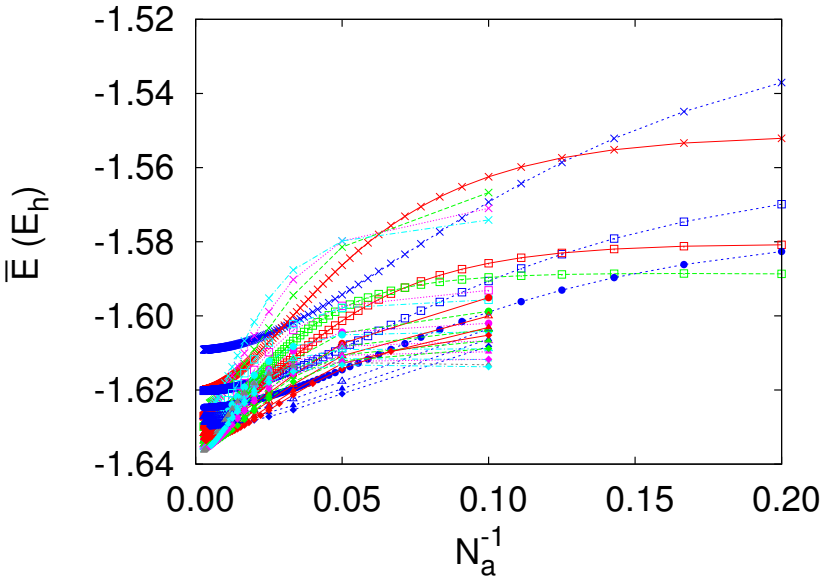

Figure 4: $\bar{E}$ vs N_a^{-1} for B1-like AlN nanorings.

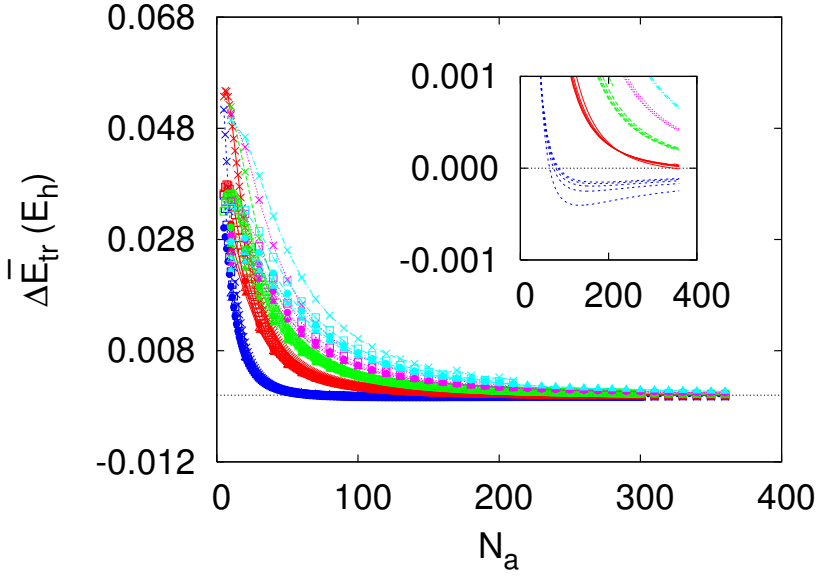

Figure 5: $\Delta\bar{E}$ vs N_a for B1-like AlN optimized nanostructures.

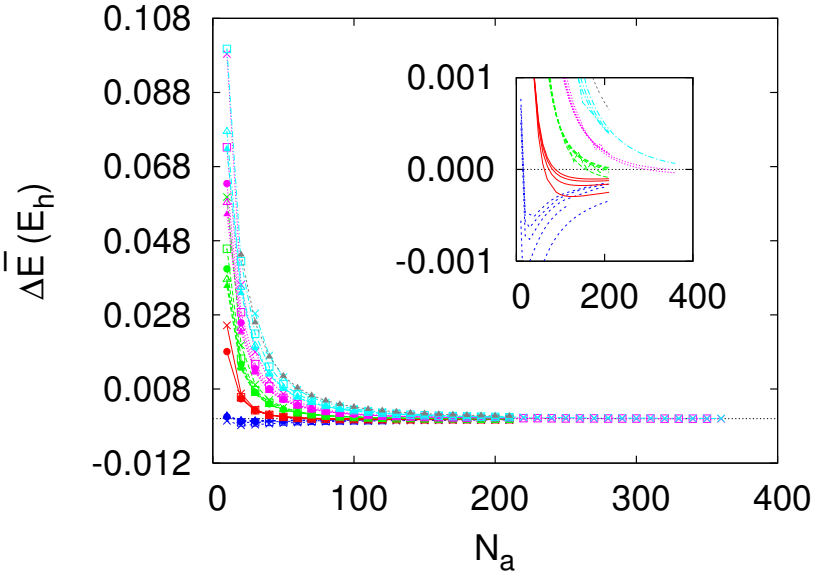

Figure 6: $\Delta\bar{E}$ vs N_a for B4-like AlN optimized nanostructures.

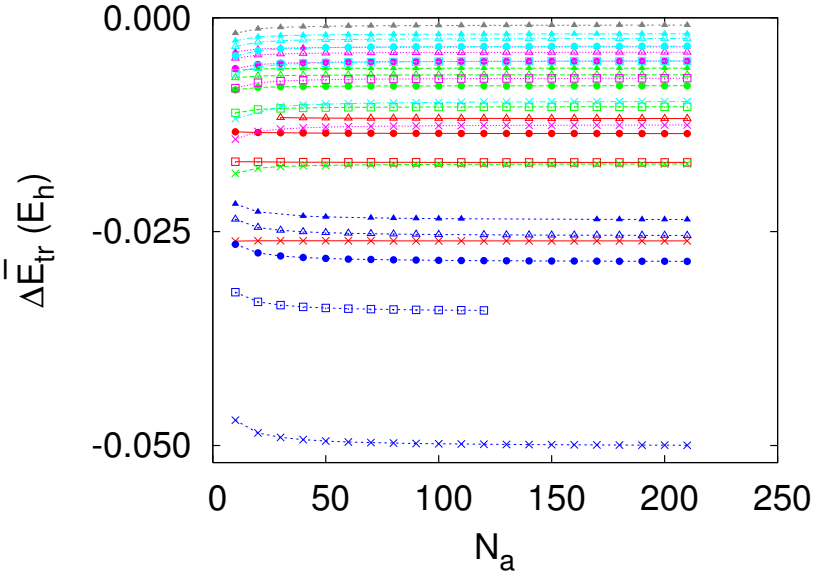

Figure 7: $\Delta\bar{E}_{tr}$ vs N_a for AlN nanobelts.

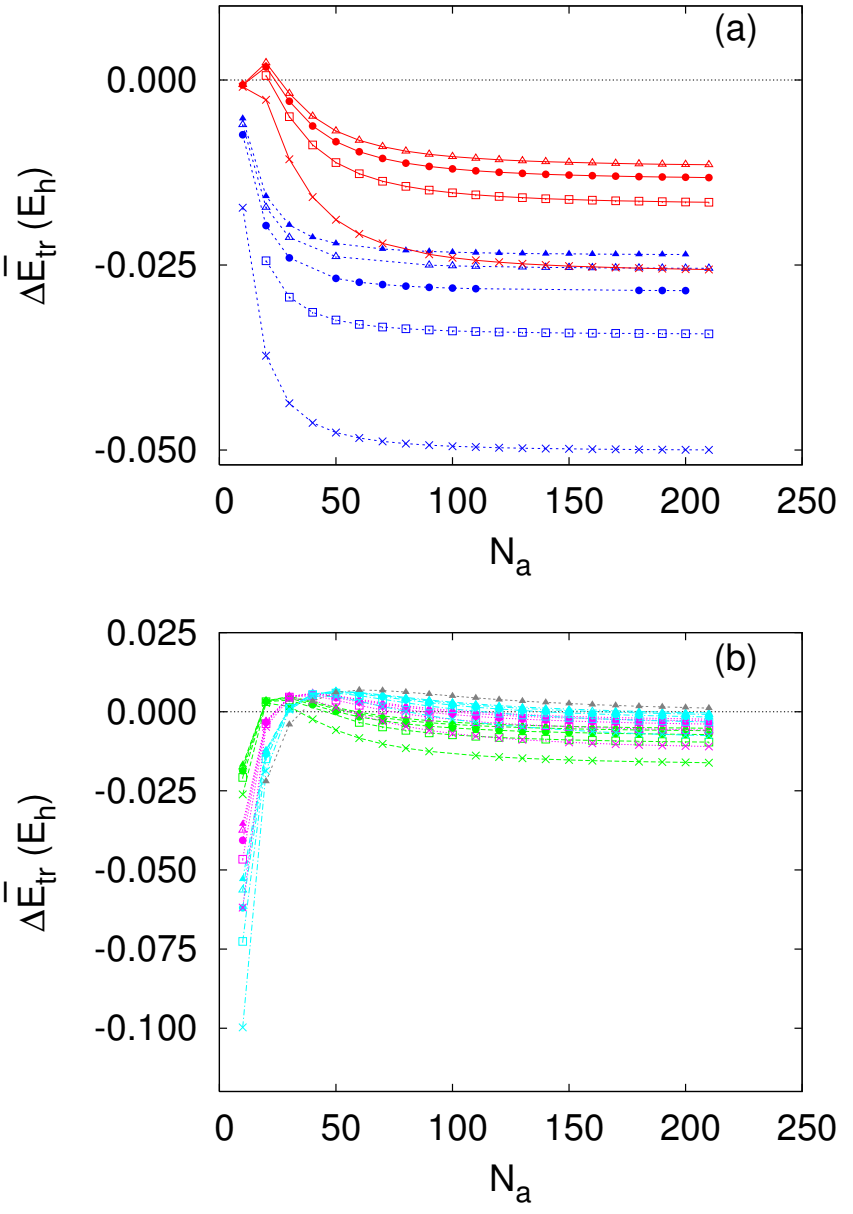

Figure 8: $\Delta\bar{E}_{tr}$ vs N_a for AlN nanorings with $N_c = 1,2$ (a) and $N_c = 3,4,5$ (b).

in the fitting) and the deformation energy contribution (i.e., the energy contribution related to the surface reduction that accompanies nanoring formation out of nanobelts) In addition, B4-like and B1-like AlN nanorings show a behavior qualitatively different, where most B1-like AlN nanorings exhibit a local maximum at small N_a values. In consequence, N_a values close to the local maximum are not included in fitting Eq. 25. In Tab. 5, $\bar{E}(\infty,N_b,N_c)$ values are shown for B4-like and B1-like AlN nanorings which are found similar to $\bar{E}(\infty,N_b,N_c)$ for B4-like and B1-like AlN nanobelts, respectively. In fact, small differences between them are probably due to either fitting or numerical errors. Following a procedure analogous to the previously described for nanobelts (see Eq. 21, Eq. 22, Eq. 23 and Eq. 24), the $\bar{E}(crystal)$ values for the B_k crystal structure are found to be $-1.6472\,E_h$ and $-1.6471\,E_h$ for data obtained for *Oxy* and *Oxz* infinite planes, respectively. Also, the $\bar{E}(crystal)$ value for the B1 crystal structure is found as $-1.6434\,E_h$.

Table 5: $\bar{E}(\infty,N_b,N_c)$ values for B4-like and B1-like AlN nanorings.

$\bar{E}(\infty,N_b,N_c)$ (E_h)				$\bar{E}(\infty,N_b,N_c)$ (E_h)			
N_b	N_c	B4	B1	N_b	N_c	B4	B1
1	1	-1.5590	-1.6091	4	1	-1.6017	-1.6272
1	2	-1.5941	-1.6204	4	2	-1.6201	-1.6319
1	3	-1.6077	-1.6247	4	3	-1.6274	-1.6340
1	4	-1.6147	-1.6271	4	4	-1.6312	-1.6353
1	5	-1.6190	-1.6293	4	5	-1.6337	-1.6363
2	1	-1.5861	-1.6202	5	1	-1.6051	-1.6288
2	2	-1.6103	-1.6273	5	2	-1.6225	-1.6330
2	3	-1.6198	-1.6302	5	3	-1.6290	-1.6349
2	4	-1.6248	-1.6319	5	4	-1.6327	-1.6361
2	5	-1.6279	-1.6336	5	5	-1.6350	-1.6370
				5	6	-1.6364	
3	1	-1.5962	-1.6247	6	1		-1.6298
3	2	-1.6167	-1.6302	6	2		-1.6338
3	3	-1.6247	-1.6326	6	3		-1.6356
3	4	-1.6292	-1.6342	6	4		-1.6374
3	5	-1.6317	-1.6356	6	5		-1.6382

We analyze now the critical sizes at which the periodic nanorings become more stable than the periodic nanobelts. Let us define $\Delta\bar{E}(N_a,N_b,N_c) = \bar{E}_{ring}(N_a,N_b,N_c) - \bar{E}_{belt}(N_a,N_b,N_c)$, where $\bar{E}_{ring}$ and $\bar{E}_{belt}$ are the energies per unit formula for nanorings and nanobelts obtained from the same initial phase. In Fig. 5 and Fig. 6, $\Delta\bar{E}$ vs

Table 6: Critical (N_a,N_b,N_c) values for nanobelt⇌nanoring interconversion for B1-like and Bk-like AlN optimized nanostructures.

B1						B$_k$											
N_c	N_b	N_a	N_c	N_b	N_a	N_c	N_b	N_a	N_c	N_b	N_a	N_c	N_b	N_a	N_c	N_b	N_a
1	1	66-67	2	1	340-350	1	1	8-9	2	1	62-63	3	1	157-158	4	1	294-295
1	2	75-76	2	2	>360	1	2	6-11	2	2	73-74	3	2	184-185	4	2	344-345
1	3	80-81	2	3	>360	1	3	10-12	2	3	81-82	3	3	205-206	4	3	>360
1	4	80-90	2	4	>360	1	4	11-13	2	4	87-88	3	4	220-230	4	4	>360
1	5	80-90	2	5	>360	1	5	13-14				3	5	230-240	4	5	>360

N_a is depicted for B1-like and B4-like AlN optimized nanostructures, respectively. The critical (N_a,N_b,N_c) values for the nanobelt⇌nanoring interconversion for B1-like and B4-like AlN optimized nanostructures are shown in Tab. 6. As found for the $\bar{E}$ vs N_a^{-1} map in B1-like AlN nanorings, $\Delta\bar{E}$ vs N_a shows a local maximum (except when $N_c = 1$) before the nanobelt→nanoring interconversion for B1-like AlN nanostructures. However, $\bar{E}$ vs N_a^{-1} doesn't exhibit these local maxima for B4-like nanostructures. The N_a critical value for the nanobelt⇌nanoring interconversion depends on the N_b and N_c values. The increase in the N_a critical value when N_c grows is steeper when N_b grows. Since both unit cells are orthogonal for AlN nanostructures and the Oy axis is selected normal to the nanoring plane, the Ob axis matches the Oy axis and, therefore, is normal to the nanoring plane. Thus, the dependence of the N_a critical value on N_b and N_c makes it clear that bending of nanobelts is more difficult when one increases their thickness (i.e., the N_c value) than when one increases their width (i.e. the N_b value). On the other hand, the B4-like nanobelt⇌nanoring interconversion appears at smaller both energies and (N_a,N_b,N_c) values if one compares it to the B1-like nanobelt⇌nanoring interconversion. This is in agreement with experimental results, where most AlN nanorings are found to be B4-like.

Finally, we analyze the B1⇌B4 phase transition for nanobelts and nanorings. Let us define $\Delta\bar{E}_{tr}(N_a,N_b,N_c) = \bar{E}_{\mathrm{B1}}(N_a,N_b,N_c) - \bar{E}_{\mathrm{B4}}(N_a,N_b,N_c)$, where $\bar{E}_{\mathrm{B1}}$ and $\bar{E}_{\mathrm{B4}}$ are the energies per unit formula for the equivalent (i.e., those displaying the same (N_a,N_b,N_c) values) B1-like and B4-like nanocrystals, respectively. The B1-like nanostructure is thermodynamically more stable if $\Delta\bar{E}_{tr} < 0$, while the contrary is true if $\Delta\bar{E}_{tr} > 0$. In Fig. 7 and Fig. 8, $\Delta\bar{E}_{tr}$ vs N_a is depicted for the optimized AlN nanobelts and nanorings, respectively. In Fig. 7, B1-like AlN nanobelts are more stable than B4-like AlN nanobelts in all the cases considered. However, $\Delta\bar{E}_{tr}$ increases when one increases nanobelt size and, therefore, the difference in stability between both phases decreases to favor the B4 phase. Moreover, $\Delta\bar{E}_{tr}$ depends strongly on the N_b and N_c values, while it depends weakly on the N_a values. Thus,

it seems that the width and the thickness of the nanobelts play an important role in the stability difference between both phases. The B1⇌B4 phase transition occurs at different N_a critical values as N_b ans N_c increase. As shown in Fig. 8 M_a seems to be more important factor in nanorings than in nanobelts. This may be rationalize if we examine the deformation energy contribution to the ring energy. Since B4-like nanostructures have higher a lattice parameter than B1-like nanostructures, the former have bigger lengths than the latter for the same N_a value. Since B4-like nanostructures have a lower c lattice parameter than B1-like nanostructures, B4-like nanostructures have smaller thickness than B1-like nanostructures with the same N_c value. Since the deformation energy is inversely proportional to the length and directly proportional to thickness. This contribution is a more significant barrier for B1-like nanostructures than B4-like ones. However, the deformation energy contribution can't explain the existence of the local maximum in $\Delta\bar{E}_{tr}$ vs N_a, which is related to the existence of the local maximum in $\bar{E}$ vs N_a^{-1} in B1-like AlN nanorings. As in nanobelts, $\Delta\bar{E}_{tr}$ increases when one increases the nanoring size.

4 Conclusions

The periodic cluster model, initially designed for the simulation of periodic clusters with parallelepipedic shape (i.e., nanocrystals), has been extended in this work simulate of nanobelts and nanorings. Further, other nanostructures could be easily included by means of a coordinate transformation similar to that described in Eq. 13.

This extension of the PC model has been implemented into an atomistic pair potential simulation code, together with an interaction model that we have developed for AlN. Through these, we have simulated a number of AlN nanobelts and nanorings. In agreement with our previous simulations, our results predict a non-buckled structure, similar to the B_k graphitic-like structure displayed by e.g. bulk BN, instead of the buckled wurtzite-like structure (B4) displayed by bulk AlN. It is argued that the polar, buckled structure will eventually overcome the non-buckled structure for a given threshold size. Although we cannot give reliable number for the buckling threshold size, this behavior can be experimentally tested: since the B_k bulk structure does display a symmetry center and is non-polar, non-buckled nanocrystals should have characteristic diffraction patterns, quite different from the polar, non-centrosymmetric, buckled ones.

We have computed the macroscopic limit for AlN nanobelts and nanorings. There is a good agreement between the ideal crystal energy obtained from both macroscopic limit extrapolated values in nanostructures and the actual crystalline value. In addition, the lattice parameters also tend to the ideal crystal values in the macroscopic limit. Because one uses the same pair potentials to evaluate the energy for

both nanostructures and the crystal, these results are a useful test to confirm that the extension of PC model is working in a right way.

We have analyzed the critical sizes at which AlN nanorings become more stable than AlN nanobelts. Our results are in agreement with experimental results where most AlN nanorings are found as B4-like nanorings.

We have also studied the B1$\rightleftharpoons$B4 phase transition for AlN nanobelts and nanorings. For nanobelts, it seems that the width and the thickness play an important role in the stability difference between both phases. For nanorings, the N_a value plays a more important role than for nanobelts because of the deformation energy contribution to the nanoring energy.

In addition to the intrinsic value of the results presented, the periodic cluster model suggests several areas for future work. On the one hand, our somewhat crude pair potential model might be substituted for more accurate ways of evaluating the potential energy surface. Although the computational cost will increase, and the range of sizes available will decrease, other interesting information like the electronic behavior might be obtained. On the other hand, neglecting the geometric surface relaxation can be a very important limitation in some cases. However, a generalized periodic cluster scheme can be sketched in which the strictly 3D periodic nanostructure is surrounded by 2D periodic slabs representing the surfaces, these in turn by 1D periodic rods representing edges, and explicit clusters representing vertices; although its dimensionality will be somewhat larger, it will still maintain the same order of magnitude as that in the 3D periodic nanostructure.

Acknowledgement: This research has been funded by the Spanish Ministerio de Educación y Ciencia CTQ2012-31174 and CSD2007-00045 MALTA-CONSOLIDER. We dedicate this work to the memory of our late colleague and friend, Prof. Miguel Álvarez Blanco.

References

Alivisatos A. P.; (1996): Perspectives on the Physical Chemistry of Semiconductor Nanocrystals. *J. Phys. Chem.*, vol 100, pp 13226.

Belyanin B. F.; Bouilov L. L.; Zhirnov V. V.; Kamenev A. I.; Kovalskiji K. A.; Spitsyn B. V. (1999): Application of aluminum nitride films for electronic devices. *Diam. Relat. Mater*, vol 8, pp 369.

Beberwyck B. J.; Alivisatos A. P.; (2012): Ion Exchange Synthesis of III-V Nanocrystals. *J. Am. Chem. Soc.*, vol 134, pp 19977.

Born M.; Mayer J. (1932): Lattice theory of ionic crystals. *Z. Phys.*, vol 75, pp 1.

Choi C. L.; Alivisatos A. P.; (2010): From Artificial Atoms to Nanocrystal Molecules: Preparation and Properties of More Complex Nanostructures. *Annu. Rev. Phys. Chem.*, vol 61, pp 369.

Costales A.; Blanco M. A.; Martín Pendás A.; Kandalam A. K.; Pandey R. (2002): Chemical bonding in group III nitrides. *J. Am. Chem. Soc.*, vol 124, pp 4116.

Costales A.; Kandalam A. K.; Pandey R. (2003): Theoretical Study of Neutral And Anionic Group III Nitride Clusters: M_nN_n (M=Al, Ga And In; n=4-6). *J. Phys. Chem. B*, vol 107, pp 4508.

Costales A.; Blanco M. A.; Francisco E:; Pandey R.; Martín Pendás A. (2005): Evolution of the properties of Al_nN_n. *J. Phys. Chem. B*, vol 109, pp 24352.

Costales A.; Blanco M. A.; Francisco E.; Martín Pendás A.; Pandey R. (2006): First Principles study of neutral and anionic (medium-size) aluminum nitride clusters: Al_nN_n, $n = 7 - 16$. *J. Phys. Chem. B*, vol 110, pp 4092.

Costales A.; Blanco M. A.; Francisco E.; Solano C. J. F.; Martín Pendás A. (2008): Theoretical simulation of AlN nanocrystals. *J. Phys. Chem. C*, vol 112, pp 6667.

Dick B. J.; Overhauser A. W.; (1958): Theory of the dielectric constants of alkali halide crystals. *Phys. Rev.*, vol 112, pp 90.

Duan J.; Yang S.; Liu H.; Gong J.; Huang H.; Zhao X.; Tang J.; Zhang R.; Du Y. (2005): AlN nanorings *J. Cryst. Growth*, vol 283, pp 291.

Francisco E. (2004): *Internal report, Universidad de Oviedo*.

Francisco E. (2005): *The Cluster program, Universidad de Oviedo*.

Grünwald M.; Rabani E.; Dellago C.; (2004): Mechanisms of the wurzite to rocksalt transformation in CdSe nanocrystals. *Phys. Rev. Lett.* vol 96, pp 255701.

Grünwald M.; Dellago C.; Geissler P. L.; (2007): An efficient transition path sampling algorithm for nanoparticles under pressure. *J. Chem. Phys.* vol 127, pp 154718.

Hill T. L. (1994): *Thermodynamics of small systems (Parts I and II)*. Dover Publications, Inc.

Huggins M. L.; Mayer J. (1933): Interatomic distances in crystals of the alkali halides. *J. Chem. Phys.*, vol 1, pp 643.

Kandalam A. K.; Blanco M. A.; Pandey R. (2002): Theoretical Study of Al_nN_n, Ga_nN_n, and In_nN_n ($n = 4,5,6$) Clusters. *J. Phys. Chem. B*, vol 106, pp 1945.

Kodiyalam S.; Kalia R. K.; Nakano A.; Vashishta P. (2004): Multiple Grains in Nanocrystals: Effect of Initial Shape and Size on Transformed Structures Under Pressure. *Phys. Rev. Lett.* vol 93, pp 203401.

Kao J.; Bai P.; Lucas J. M.; Alivisatos A. P.; Ting X.; (2013): Size-Dependent assemblies of nanoparticle mixture in thin films. *J. Am. Chem. Soc.*, vol 135, pp 1680.

Kong X. Y.;, Ding Y.; Yang R. S.; Wang Z. L. (2004): Single-Crystal Nanorings Formed by Epitaxial Self-Coiling of Polar Nanobelts. *Science*, vol 303, pp 1348.

Liu D.; Nocedal J. (1989): On the limited memory BFGS method for large scale optimization. *Mathematical Programming B*, vol 45, pp 503.

Mayer J.; Levy R. B. (1933): The lattice energies of the cuprous halides. *J. Chem. Phys.*, vol 1, pp 647.

Morgan B. J.; Madden P. A.; (2004): Pressure-Driven Sphalerite to Rock Salt Transition in Ionic Nanocrystals: A Simulation Study. *Nano. Lett.*, vol 4, pp 1581.

Morgan B. J.; Madden P. A.; (2006): A molecular dynamics study of structural relaxation in tetrahedrally coordinated nanocrystals. *Phys. Chem. Chem. Phys.* vol 8, pp 3304.

Morgan B. J.; Madden P. A.; (2006): Pressure-Driven Phase Transitions in Crystalline Nanoparticles: Surface Effects on Hysteresis. *J. Phys. Chem. C* vol 111, pp 6724.

Morgan B. J.; (2010): First-principles study of epitaxial strain as a method of B4-BCT stabilization in ZnO, ZnS, and CdS. *Phys. Rev. B* vol 82, pp 153408.

Nakamura S. (1996): *Proceedings of International Symposium on Blue Laser and Light Emitting Diodes* A. Yoshikawa, K. Kishino, M. Kobayashi, T. Yasuda, Eds.; Chiba University Press, pp 119.

Nocedal J. (1980): Updating quasi-Mewton matrices with limited storage. *Math. Comput.*, vol 35, pp 773.

Serrano J.; Rubio A.; Hernández E.; Muñoz A.; Mújica A. (2000): Theoretical study of the relative stability of structural phases in group-III nitrides at high pressures. *Phys. Rev. B*, vol 62, pp 16612.

Solano C. J. F. (2009): *PhD Thesis* Universidad de Oviedo.

Solano C. J. F.; Costales A,; Francisco E.; Martín Pendás A.; Blanco M. A.; Lau K. C.; He H.; Pandey R. (2008): Buckling in wurzite-like AlN nanostructures and crystals: Why nano can be different. *CMES*, vol 24, pp 143.

Wang Z.; Tait K.; Zhao Y.; Schiferl D.; Zha C.; Uchida H.; Downs R. T (2004): Comparative studies of structural transition between AlN nanocrystals and nanowires. *J. Phys. Chem. B*, vol 108, pp 11506.

Wang Z. L. (2004): Nanostructures of zinc oxide. *Mater. Today*, vol 7, pp 26-33.